Anyang, P., Qunhui, Y., Huaiyang , Z., Fuwu, J., Hu, W., & Pancost, R. (2016). A diagnostic GDGT signature for the impact of hydrothermal activity on surface deposits at the Southwest Indian Ridge. *Organic Geochemistry*, *99*, 90-101. https://doi.org/10.1016/j.orggeochem.2016.07.001

A diagnostic GDGT signature for the impact of hydrothermal activity on surface deposits at the Southwest Indian Ridge

Anyang Pan [a, b, #], Qunhui Yang [a, *], Huaiyang Zhou [a, *], Fuwu Ji [a], Hu Wang [a], Richard D. Pancost [b]

[a] *State Key Laboratory of Marine Geology, School of Ocean and Earth Science, Tongji University, Siping Rd. 1239, Shanghai 200092,China*
[b] *Organic Geochemistry Unit, School of Chemistry, Cabot Institute, University of Bristol, Cantock's Close, Bristol BS8 1TS, UK*

* Corresponding author. Tel: +86 13918209499
E-mail address: yangqh@tongji.edu.cn (Qunhui Yang), zhouhy@tongji.edu.cn (Huaiyang Zhou)

[#] Present address: *SINOPEC Petroleum Exploration and Production Research Institute, Wuxi Institute of Petroleum Geology, 2060 Lihu Road, Wuxi, Jiangsu 213126, China*

Abstract

The impact of hydrothermal activity on wider ocean geochemistry and microbial ecology remains a topic of much interest. To explore whether hydrothermal microbial signatures are exported to surrounding marine sediments or if such organisms serve as an important source of sedimentary organic matter, we determined the distributions of glycerol dialkyl glycerol tetraether (GDGT) membrane lipids in surficial normal marine sediments, metalliferous sediments and low-temperature hydrothermal deposits at newly discovered hydrothermal fields and adjacent areas at the Southwest Indian Ridge (SWIR). The GDGTs in those samples varied significantly, evidently representing a variable influence of the hydrothermal activity. GDGT compositions of surficial background sediments in SWIR were similar to those commonly observed in marine sediments, dominated by GDGTs associated with marine planktonic archaea and especially GDGT-0 and crenarchaeol. In contrast, the GDGTs of metalliferous sediments strongly impacted by hydrothermal activity and low-temperature hydrothermal deposits were markedly different, characterized by high relative abundances of isoprenoid GDGTs (*i*GDGTs)

bearing multiple rings (yielding a higher ring index), low relative abundances of crenarchaeol, and the presence of glycerol monoalkyl glycerol tetraether lipids (GMGTs; so called 'H-tetraethers') that were absent in the normal marine sediments. Sources for these hydrothermal-specific tetraether lipids likely include methanogens and anaerobic methanotrophic archaea (GDGT-0 and GDGT-1-3, respectively), *Thermoprotei* and *Thermoplasmatales* (elevated GDGT-3-4), and other thermophilic archaea including *Methanobacteriales* (GMGTs). Deposits influenced by low-temperature hydrothermal activity also contained higher abundances of branched GDGTs (*br*GDGTs) typically attributed to soil bacteria. The more distal metalliferous sediments influenced by the neutrally buoyant plume did not contain putative hydrothermal GDGTs, having the same GDGT distribution as the background sediments. This suggests that the neutrally buoyant plume has a limited potential to directly influence the organic matter inputs to surrounding sediments, due to a rapidly waning chemosynthetic microbial contribution relative to normal marine contributions as the plume dispersed and was diluted.

Keywords: tetraethers; organic matter; Southwest Indian Ridge; hydrothermal activity; chemosynthetic microbial contribution

1. Introduction

In 1977, scientists diving in the submersible *Alvin* made a stunning discovery on the bottom of the Galapagos Rift in the eastern Pacific Ocean, where seafloor hydrothermal activity and a novel ecosystem were observed (Corliss et al., 1979). Since then, these discoveries have changed our understanding of Earth and life, and 532 active and 56 inactive submarine hydrothermal vent fields have been discovered (Beaulieu et al., 2013). The vent deposits are known to harbor high-

biomass benthic communities with chemosynthetic primary producers and other microbes serving as the foundation of the food web (Govenar, 2012). They can use chemical energy, derived from mixing of reduced chemicals such as CH_4, H_2S, H_2 and metals in hydrothermal fluids with oxygenated seawater. Black smoker hydrothermal vents exude fluids with μM–mM Fe concentrations (Von Damm et al., 1985; Douville et al., 2002), which can be as much as seven orders of magnitude greater than typical deep ocean dissolved Fe of ~0.2–0.8 nM (Klunder et al., 2011; Noble et al., 2012; Hatta et al., 2015). Low concentrations of the micronutrient iron in seawater are known to limit primary production and nitrogen fixation in large regions of the global ocean, but recent research demonstrates that dissolved iron from hydrothermal vents can be transported thousands of kilometers from the venting site, contributing to the marine dissolved iron inventory, especially in the abyssal ocean (Toner et al., 2012; Fitzsimmons et al., 2014). In this and other areas, it remains vital to examine the impact of hydrothermal activity on the wider ocean geochemistry and microbial ecology.

Diverse microbiological investigations, often involving culture-independent molecular studies of 16S rRNA but also enrichment and isolation studies, have been used to examine microbial diversity in deep-sea hydrothermal vent systems (e.g. Takai et al., 2001; Kormas et al., 2006; Sogin et al., 2006; Jaeschke et al., 2012; Reeves et al., 2014). However, these approaches have inherent limitations, such as inconsistent DNA recovery, kinetic biases inherent in polymerase chain reaction, and the need to develop sepecific and appropriate primers and probes (Chowdhury and Dick, 2012). Organic geochemical approaches also have limitations but can offer a complementary view on microbial community structures since they do not require the culturing of microorganisms, are quantitative and reproducible, and can integrate a longer time window than nucleic acid based researches (Mrozik et al., 2014). There has been some research

on lipid biomarkers in hydrothermal fluids, sulfides, oxides, hydrothermally heated sediments and organisms from the Mid-Atlantic Ridge, Arctic Mid-Ocean Ridge, East Pacific Rise, Guyamas Basin spreading center and other hydrothermal systems (e.g. Schouten et al., 2003; Phleger et al., 2005; Blumenberg et al., 2012; Hu et al., 2012; Jaeschke et al., 2012; Kellermann et al., 2012; Méhay et al., 2013; Jaeschke et al., 2014; McCollom et al., 2015), including investigations of intact polar lipids (IPLs) (Gibson et al., 2013; Reeves et al., 2014), and these have helped reveal the structure and function of chemosynthetic systems. Since Archaea have high growth temperatures, up to 121 °C (Kashefi and Lovley, 2003), and are widespread in hydrothermal systems, there have been increasing investigations of archaeal membrane lipids in submarine and terrestrial hydrothermal sites in recent years (e.g. Schouten et al., 2003; Pearson et al., 2004, 2008; Pancost et al., 2005, 2006; Boyd et al., 2011; Kaur et al., 2011, 2015; Jaeschke et al., 2012; Kellermann et al., 2012; Boyd et al., 2013; Gibson et al., 2013; Lincoln et al., 2013; Méhay et al., 2013; Jaeschke et al., 2014; Reeves et al., 2014).

Here we survey the glycerol dialkyl (and monoalkyl) glycerol tetraether (GDGT and GMGT) membrane lipid distributions (Fig. 1) at the Southwest Indian Ridge, an area where little work has been done using either microbiological or organic geochemical approaches (see below). We examined a combination of hydrothermal deposits and metalliferous (plume) deposits, and used these to obtain a lipid profile and insights into the archaeal community in the hydrothermal field. This allowed us to test whether hydrothermal activity impacted the organic matter (OM) composition of surrounding surface sediments.

2. Samples and methods

2.1. Study area and samples

The SWIR is the ultraslow spreading part of the Indian ridge and the sole modern migration pathway between the diverse vent fauna of the Atlantic and Pacific oceans (German et al., 1998; Zhou and Dick, 2013). It is an area of interest, therefore, with respect to the characterization, distribution and migration of submarine microbes, and potentially for the discovery of new deep sea communities (Rogers et al., 2012; Tao et al., 2012; Amon et al., 2015; Chen et al., 2015a, 2015b, 2015c, 2015d). Molecular biological (Peng et al., 2011; Li et al., 2013; Li et al, 2015), element geochemistry and mineralogical (Tao et al., 2011, 2012; Cao et al., 2012) studies have been conducted in the SWIR hydrothermal field, but studies of lipid biomarkers and related biogeochemical processes are rare and focused on hydrocarbons and fatty acids in hydrothermal barnacle shells and sulfides (Huang et al., 2014; Lei et al., 2015).

The samples described in this paper were recovered from Dragon Vent Field (49°39′ E, 37°47′ S), a nearby inactive field (50°28′ E, 37°39.50′ S) and surrounding areas during the DY115-20 and DY115-21 expeditions of R/V Da Yang Yihao in 2009 and 2010 (Fig. 2). Dragon Vent Field, the first active hydrothermal vent to be discovered in the SWIR was found using a remotely operated vehicle from Woods Hole Oceanographic Institution (Tao et al., 2007), at a depth of 2760 m. It harbors many active and inactive sulfide chimneys with mussels, barnacles, sea cucumbers and gastropods (Copley, 2011; Rogers et al., 2012; Tao et al., 2012; Cole et al., 2014). Abundant bivalve and gastropod shells were also observed at the inactive field (~ 200 × 125 m in extent, approximately 73 km away from Dragon Vent Field, at a depth of 1770 m) (Tao et al., 2012).

All samples were collected by television grab and divided into three categories (see Supporting Information Table S1) according to the results of mineral and element geochemistry (Pan, 2015): (1) background sediments containing abundant foraminifera detritus, apparently

uninfluenced by hydrothermal activity; (2) three metalliferous sediments influenced by various degrees of hydrothermal activity depending on the distance from the hydrothermal vent; and (3) low-temperature hydrothermal deposits enriched in Fe and/or Si, noting that even though these are 'low-temperature' hydrothermal deposits, precipitation temperatures are greater than background sediments of SWIR, ranging between 38.3 to 81.8 °C based on the deduction of oxygen isotopic compositions of amorphous silica in low-temperature hydrothermal deposits from SWIR (Li et al., 2013). Typical samples from the same studied sites (SW35, SW33 and SW36) have been analysed for molecular biology (Peng et al., 2011; Li et al., 2013).

The three metalliferous sediments can be classified on the basis of their mineral and element compositions. M-T1 sediments, the furthest from the hydrothermal field, with neutrally buoyant plume fall-outs mixed in, have abundant calcite and slightly higher contents of Fe, Cu and Zn than background sediments. M-T2 sediments, with some oxides mixed in, mainly nontronite and two-line-ferrihydrite, have relatively higher contents of Fe, Mn, Cu and Zn than M-T1, mainly impacting by low-temperature hydrothermal activity. M-T3 sediments have highest Cu and Zn contents, and abundant goethite, representing a direct influence from high-temperature hydrothermal activity (Dias et al., 2008).

2.2. Bulk organic parameters

Total carbon (TC) and inorganic carbon (IC) were determined using a Carlo Erba EA1108 Elemental Analyzer and a modified Coulomat 702 analyzer, respectively. Total organic carbon (TOC) concentrations were determined by the difference between TC and IC. All reported TOC values were the means of duplicate measurements. Carbon isotopic compositions of TOC ($\delta^{13}C_{TOC}$) were obtained after pretreatment with 4 mol/L HCl with a Flash EA 1112 HT-Delta V

Advantage (Thermo Company). The $\delta^{13}C_{TOC}$ [‰ Vienna Pee Dee Belemnite, VPDB] error was ±0.2‰.

2.3. Lipid analysis

Two methods were used successively to extract and separate fractions in samples of different types. Metalliferous sediments (M-T2 and M-T3) and low-temperature hydrothermal deposits were processed with method 1, using a modified Bligh-Dyer extraction (Bligh and Dyer, 1959) and fractionation protocol based on Dickson et al. (2009). After freeze-drying, about 15 g of each sample were solvent extracted with a culture tube using a single-phase mixture comprised of methanol, chloroform, and aqueous 50 mM phosphate buffer water (pH 7.4) in the volume ratio of 2:1:0.8 (6×). The phases were separated by addition of chloroform and buffer water. The organic phase containing the lipids was collected, and activated copper turnings were added to the extracts for 24 hours to remove elemental sulfur. An aliquot of the total extract was separated into three fractions on a silica column. Fractionation was achieved with chloroform:acetic acid (100:1, v:v), acetone and methanol as eluents to recover simple core lipids (CL), glycolipids (GL) and phospholipids (PL), respectively. The CL fraction was subsequently eluted through a silica column with chloroform saturated with ammonium hydroxide and chloroform:acetic acid (100:1, v:v) to separate neutral components and free fatty acids. GDGTs were not detected in neutral components of the CL fraction based on method 1 and it appears that they were eluted in the GL fraction; previous workers have observed similar behavior and it seems that this method is more appropriate for bacterial membrane lipids (Pitcher et al., 2009).

Method 2 was used for the background sediments and M-T1. About 15 g sediments were

ultrasonically extracted three times with methanol, dichloromethane:methanol (1:1, v:v) and dichloromethane, respectively (Schouten et al., 2002). The total lipid extract was subsequently separated using a fractionation protocol derived from Oba et al. (2006) and Pitcher et al. (2009), using a silica column and eluting with hexane:ethyl acetate (3:1, v:v), ethyl acetate and methanol to yield CL, GL and PL fractions, respectively.

For both methods, to remove polar head groups, 5% HCl in methanol was added to the GL and PL fractions which were then heated at 100 °C for 3 h, after which the organic phase was extracted with double distilled water and chloroform. Because the CL fraction was eluted in the GL fraction in method 1, we have combined GDGT abundances and distributions in the CL and GL fractions for all samples, and discuss only summed CL+GL distributions in order to make an effective comparison among sediments of different types. We also note that silica gel column chromatography separations used in this study are always associated with significant losses of IPL-GDGTs (Lengger et al., 2012); because this likely differs among methodologies, it is inappropriate to compare concentrations even within the constraints of this study – and certainly with other studies. Therefore, this paper focuses soley the distributions of tetraether lipids and how they differ among sediments of different types. This approach should be robust as several studies have shown that although concentrations are methodologically dependent, tetraether lipid distributions are consistent (e.g. Schouten et al., 2009, 2013a). To test this further, we processed one sample with both methods and distributions of GDGTs and GMGTs were similar (see Supporting Information Table S3).

Due to the different methods, we do not discuss the potentially fossil vs living signals (core vs intact polar GDGTs). However, we do note that phospholipid distributions (data shown in Supporting Information Table S4) generally show the same relationships among different

192 sediment types as observed for the combined CL+GL fractions discussed below. This is likely a
193 fruitful avenue of future research.

194 Aliquots of all fractions were analysed by high performance liquid chromatography/
195 atmospheric pressure chemical ionisation-MS (HPLC/APCI-MS, Agilent 1100 series) equipped
196 with an autoinjector and Chemstation software (Agilent) in a modification of the procedure of
197 Hopmans et al. (2000) and then Schouten et al. (2007a). Fractions were dissolved in
198 hexane:isopropanol (99:1, v/v) and filtered through 0.45 μm mesh PTFE. Separation of GDGTs
199 was achieved on an Alltech Prevail Cyano column (2.1 mm i.d. × 150 mm, 3 μm) maintained at
200 30 °C with a flow rate of 0.2 ml/min. Injection volume was 20 μl. GDGTs were eluted
201 isocratically with 99% hexane and 1% isopropanol for 7 min, followed by a linear gradient to
202 1.3% isopropanol at 30 min, to 1.6% isopropanol at 35 min, then increasing to 10% isopropanol
203 at 36 min and kept for 8 min, finally equilibrating with 1% isopropanol for 13 min before the
204 next injection. After each two analyses, the column was cleaned by back-flushing
205 hexane:isopropanol 99:1 (v:v) for 7 min and then rinsed by a linear gradient from 90:10 (v:v)
206 hexane:isopropanol to 99:1 (v:v) hexane:isopropanol within 14 min and equilibrated with 1%
207 isopropanol at 30 min. Conditions for APCI-MS were as follows: vaporizer temperature 380 °C,
208 drying gas (N_2) flow 6 l/min and temperature 200 °C, capillary temperature 282 °C, corona
209 discharge current 3 μA. GDGTs were detected in selected ion monitoring (SIM) mode and were
210 semi-quantified by an internal synthetic C_{46} tetraether standard, based on the procedure of
211 Huguet et al. (2006) and Schouten et al. (2007a).

212 The branched isoprenoid tetraether (BIT) index, a proxy for terrestrial OM input, was used
213 as defined by Hopmans et al. (2004):

214 $$BIT = \frac{[GDGT-I]+[GDGT-II]+[GDGT-III]}{[GDGT-I]+[GDGT-II]+[GDGT-III]+[Cren]} \quad (1)$$

, where numbers refer to individual GDGT structures shown in Figure 1. The methylation of branched tetraether (MBT) and cyclization of branched tetraethers (CBT) ratios were used as defined by Weijers et al. (2007):

$$MBT = \frac{([GDGT-I]+[GDGT-Ia]+[GDGT-Ib])}{\Sigma[all\ branched\ GDGTs]} \quad (2)$$

$$CBT = -\log(([GDGT-Ia]+[GDGT-IIa])/([GDGT-Ia]+[GDGT-IIa])) \quad (3)$$

The ring index (RI) was defined based on Pearson et al. (2004):

$$RI = \frac{1\times[GDGT-1]+2\times[GDGT-2]+3\times[GDGT-3]+4\times[GDGT-4]}{[GDGT-1]+[GDGT-2]+[GDGT-3]+[GDGT-4]} \quad (4)$$

The methane index (MI) was used as defined by Zhang et al. (2011):

$$MI = \frac{[GDGT-1]+[GDGT-2]+[GDGT-3]}{[GDGT-1]+[GDGT-2]+[GDGT-3]+[Cren]+[Cren']} \quad (5)$$

The tetraether index of tetraethers consisting of 86 carbons (TEX_{86}) was used as defined by Schouten et al. (2002):

$$TEX_{86} = \frac{[GDGT-2]+[GDGT-3]+[Cren']}{[GDGT-1]+[GDGT-2]+[GDGT-3]+[Cren']} \quad (6).$$

3. Results

3.1. Total organic carbon and carbon isotopic composition

The TOC contents and $\delta^{13}C_{TOC}$ values varied among the different sediment types

(Supporting Information Table S1 and Fig. 3). Background sediments had the highest TOC contents (1.2% average) and relatively heavy $\delta^{13}C_{TOC}$ values (-22.1‰ average). Low-temperature hydrothermal deposits had the lowest TOC contents (0.13% average) and more depleted $\delta^{13}C_{TOC}$ values (-24.8‰ average). In the metalliferous sediments, TOC contents and $\delta^{13}C_{TOC}$ values in M-T1 were similar to the background sediments, whereas those parameters in M-T2 were close to those of the low-temperature hydrothermal deposits. TOC contents were slightly higher in M-T3 than M-T2 and low-temperature hydrothermal deposits, but similar $\delta^{13}C_{TOC}$ values.

3.2. Tetraether lipid distributions

GDGTs observed in the SWIR samples include a range of isoprenoidal GDGTs (*i*GDGTs) bearing 0 to 4 cyclopentyl moieties as well as crenarchaeol and its regioisomer; a suite of the unusual "H-shaped" glycerol monoalkyl glycerol tetraethers (GMGTs, up to four cyclopentyl moieties but mainly GMGT-0); and surprisingly, branched GDGTs, often in high abundances (*br*GDGTs, including GDGT III-IIIb, GDGT II-IIb, GDGT I-Ib). Trace amounts of glycerol trialkyl glycerol tetraether (GTGT-0; i.e. with one biphytanyl and two phytanyl components and no cyclopentyl moities) were also detected in the low-temperature hydrothermal deposits (Supporting Information Table S2).

Among the *i*GDGTs, GDGT-0 and crenarchaeol were dominant in background sediments and M-T1, with crenarchaeol percentages typically being 40-50%. Proportions of GDGTs 1-3 were lower and distributions were overall similar to other marine sediments (Schouten et al., 2013b). The proportion of crenarchaeol was markedly lower in M-T2, M-T3 and low-temperature hydrothermal deposits, largely due to higher proportions of GDGTs 0-3 but also

GDGT-4, which was not detected in the background sediments. The *i*GDGT distributions of M-T3 was dominated by GDGT-0 and GDGT-4 (Supporting Information Table S2).

The isoprenoidal GMGTs (*i*GMGTs) were not detected in background sediments nor in M-T1, but had high relative abundances in the low-temperature hydrothermal deposits and the metalliferous sediments strongly impacted by hydrothermal activity and close to the hydrothermal vent; in fact *i*GMGTs represent >45% of the total tetraether lipids in M-T3, in which GMGT-0 and GMGT-4 were the main components. The proportions of *i*GMGTs in M-T2 and low-temperature hydrothermal deposits were lower, but still higher than those of the other sediments, and dominated by GMGT-0.

The proportions and abundances of *br*GDGTs were very low in most background samples, M-T1 and M-T3, but markedly higher in M-T2 and low-temperature hydrothermal deposits (>15%). This yielded higher BIT indices for the latter – 0.24 to 0.69 in M-T2 and hydrothermal deposits compared to <0.10 in the other sediment types (Table 1). GDGT-III, GDGT-II and IIa were dominant compounds in most samples. However, GDGT-I was also predominant in M-T2 and low-temperature hydrothermal deposits, such that CBT and MBT indices were larger (Table 1).

In summary, tetraether lipid distributions were dominated by *i*GDGTs in all three SWIR sample categories (Table 1), but the percentages of *i*GDGTs were relatively lower in M-T2, M-T3 and low-temperature hydrothermal deposits, whereas *i*GMGTs were relatively more abundant. Branched GDGTs were also proportionally more abundant in the low-temperature hydrothermal deposits and M-T2. This results in three main groups, shown in the ternary diagram of *i*GDGTs, *i*GMGTs and *br*GDGTs (Fig. 4): Group 1 comprises background sediments and M-T1; Group 2, characterized by relatively higher percentages of *br*GDGTs, comprises some M-T2 and low-

temperature hydrothermal deposits; and Group 3, characterized by relatively higher percentages of *i*GMGTs, comprises the other M-T2 and low-temperature hydrothermal deposits as well as M-T3.

4. Discussion – Variations in Organic Matter Sources

TOC contents in SWIR background sediments were higher than the global average for deep-sea surficial sediments (0.25~0.50%, Premuzic et al., 1982). This could be associated with elevated concentrations of phytoplankton and zooplankton in the study area, which has been identified as an important carbon sequestration region (Froneman et al., 1998; Llido et al., 2005). $\delta^{13}C_{TOC}$ values of most background sediments are in the typical range of marine organic matter (-22‰ to -19‰, Fontugne and Jouanneau, 1987), indicating that organic matter of SWIR background sediments was mainly derived from autochthonous marine organisms. This is also consistent with the presence of lipid biomarkers for phytoplankton (i.e. sterols and alkenones, data not shown). The $\delta^{13}C$ values of the metalliferous sediments (except M-T1) and most of the low-temperature hydrothermal deposits were lower, consistent with relatively low $\delta^{13}C$ values for organic matter in other hydrothermal settings (e.g. Southern Mariana Trough, Kato et al., 2010; Loki's Castle, Jaeschke et al., 2012, 2014; PACMANUS, Reeves et al., 2014); this is typically attributed to the production of ^{13}C-depleted OM by chemosynthetic organisms. Intriguingly M-T1 TOC has a $\delta^{13}C$ value similar to that of background sediments, suggesting that deposition of neutrally buoyant plume material has not imparted an obvious hydrothermal OM signature to the areas far away from the hydrothermal vents.

To explore these differences in OM source and microbial ecology further we have examined the tetraether lipids of surface sediments from SWIR. Tetraether lipid distributions differ among

the normal marine sediments, metalliferous sediments and the low-temperature hydrothermal deposits. Based on the relative distributions of *i*GDGTs, *i*GMGTs and *br*GDGTs, background sediments but also M-T1 have OM sources typical of deep marine sediments, primarily GDGTs exported from overlying waters (Group 1). M-T2 and M-T3 distributions are similar to low-temperature hydrothermal deposits but can still be divided into two sub-groups: Group 2 with >11% *br*GDGTs and Group 3 with >10% *i*GMGTs.

Combined with the previous molecular biological analyses of samples from the same studied sites at SWIR (Peng et al., 2011; Li et al., 2013), likely sources of different tetraether lipid classes can be assigned. The GDGT-0/crenarchaeol, MIs and RIs all indicate that the hydrothermal deposits have additional archaeal sources compared with background sediments. Moreover, the percentages of *br*GDGTs and BIT indices, combined with unusual MBT/CBT ratios, appear to reflect in situ bacteria production.

4.1. Isoprenoidal GDGTs

The *i*GDGTs in background sediments and M-T1 of SWIR were dominated by GDGT-0 and crenarchaeol and lower contents of *i*GDGTs 1-3.This is similar to distributions in the surficial sediments from other oceans and indicates a major contribution to tetraether membrane lipids from non-thermophilic Thaumarchaeota in the marine environment (Schouten et al., 2002). TEX_{86} values in these samples were also consistent with SWIR sea surface temperatures (SSTs, http://www.ospo.noaa.gov/data/sst/contour/global.c.gif) and global calibrations (Fig. 5a; Kim et al., 2010), suggesting a predominantly allochthonous source of water-column GDGTs, which has been confirmed by recent 16s rRNA analysis (mainly Thaumarchaeota, unpublished data).

The compositions of *i*GDGTs in most metalliferous sediments and low-temperature

hydrothermal deposits, with higher contents of total *i*GDGTs 0-4 and lower contents of crenarchaeol, were different from background sediments. Some of this could be attributed to the presence of crenarchaeota *Thermoprotei* and euryarchaeota *Thermoplasmatales*, previously documented for some of these samples (Peng et al., 2011; Li et al., 2013) and known sources of *i*GDGTs 1-4 (reviewed in Pearson and Ingalls, 2013; Schouten et al., 2013b).

Additional contributions of non-pelagic archaea to the isoprenoidal GDGT pool can be ascertained by testing expected TEX_{86} indices against the RI. Group 2 and 3 sediments are both associated with high RIs, but RIs are higher for the latter and Group 2 TEX_{86} values are similar (albeit at the high end) of the background sediment range. Therefore, it appears that *i*GDGTs in Group 3 sediments – and perhaps Group 2 sediments – derive from sources additional to those that dominate normal marine sediments, presumably hydrothermal organisms.

Additionally, the *i*GDGT distributions could primarily reflect the different environmental conditions under which Group 2 and 3 sediments formed. TEX_{86} indices in marine sediments have a positive correlation with sea surface temperatures in overlying waters but generally not with pH (e.g. Schouten et al., 2002; Kim et al., 2008, 2010; Boyd et al., 2011). Other studies have also shown that temperature is an important control on the distribution of archaeal tetraether membrane lipids, with RIs increasing with growth temperature (Pearson et al., 2004; Uda et al., 2004; Elling et al., 2015; Kaur et al., 2015). Similar studies, however, have shown that pH also governs GDGT distributions in thermophilic archaea, with RI increasing as pH decreases in diverse settings (e.g. Boyd et al., 2011, 2013; Wu et al., 2013; Kaur et al., 2015).

To date, the highest temperature vent fluid observed in the Dragon vent field is 379 °C (unpublished data). Previous studies showed the $pH_{(in\ situ)}$ of the highest temperature vent fluid (> 380 °C) measured in situ with solid-state electrochemical sensors, is slightly acidic (5.1–5.4).

However, mixing of seawater with vent fluid results in seawater dominated conditions with attendant pH increases (Ding et al., 2005), such that below 121 °C, the upper temperature limit for life (Kashefi and Lovley, 2003), $pH_{(in\ situ)}$ is usually greater than 6.0, approaching neutrality (Ding et al., 2005). It is unclear if a pH range from about 6 to 8 can explain the large variations in GDGT distributions observed here due to the lack of in situ pH information. Pure culture study of marine planktonic thaumarchaeal isolates demonstrated that pH variations over a range of 7.3 to 7.9 exerted a minor influence on GDGT cyclization, however, pH might influence environmental GDGT distribution indirectly by selecting for specific thaumarchaeal lineages with distinct lipid compositions (Elling et al., 2015). Moreover, pH has been shown to be a control on RIs in other settings, albeit over a larger range. Therefore, the unusual *i*GDGT distributions in Group 2 and especially Group 3 likely reflect a range of ecological but also environmental factors, primarily dictated by temperature but possibly also related to pH variations.

Both GDGT-0 and crenarchaeol occur in marine group 1 Crenarchaeota, but only GDGT-0 appears to be produced by methanogens (Schouten et al., 2007b). The GDGT-0/crenarchaeol ratio in marine group 1 Crenarchaeota typically varies between 0.2 and 2 (Schouten et al., 2002) and ratios >2 suggest an additional source for GDGT-0 (Blaga et al., 2009). The GDGT-0/crenarchaeol ratios were <2 in background sediments and M-T1 (Group 1), whereas the ratios in some metalliferous sediments and low-temperature hydrothermal deposits (Group 3) were > 2 (Fig. 5b). Unlike RIs, greater abundances of GDGT-0 are difficult to ascribe to higher temperatures or lower pH and we instead suggest that this is evidence for an additional source, possibly methanogenic archaea. Abundant methanogens (mainly Methanosarcinale or Methanobacteriales) have been detected in some hydrothermal deposits at the same SWIR sites

(Peng et al., 2011; Li et al., 2013). However, other archaeal species cannot be excluded as contributors (e.g. Pearson et al., 2013; Schouten et al., 2013b; Villanueva et al., 2014) and we note that Archaeoglobales was also detected in these settings (Peng et al., 2011).

The GDGT-0/crenarchaeol ratios were <2 in Group 2, which could suggest a hydrothermal origin for both compounds, and crenarchaeol has been found in both terrigenous (e.g. Pearson et al., 2004; Schouten et al., 2007b; Pitcher et al., 2011) and marine hydrothermal systems (Méhay et al., 2013); alternatively, it is consistent with a smaller hydrothermal overprint of Group 2 samples (compared to Group 3), consistent with the lower RIs and TEX_{86} values.

GDGT MIs below 0.3 to 0.5 are typical of normal marine sediments, whereas MIs of sediments impacted by additional microbial inputs, including anaerobic methanotrophs, are typically >0.5 (Pancost et al., 2001a; Zhang et al., 2011). The MI of most samples of Groups 1 and 2 were < 0.3, with several background sediments in the range of 0.3~0.5; in contrast, the MIs of most Group 3 samples were > 0.6 (Fig. 5b), indicating an additional contribution. As hydrothermal plume samples collected from Dragon Vent Field have higher CH_4 contents than background water, by at least one order of magnitude (Wang et al., 2015), it seems likely that archaea involved in methane production and consumption could have contributed to the *i*GDGT signature of Group 3, affecting both MIs and %GDGT-0. However, the elevated MIs can also be explained by environmental impacts on GDGT distributions, as discussed above.

To explore these two options, we have examined other biomarker classes. Archaeol has always been found in association with anaerobic methane-oxidising Archaea (Blumenberg et al., 2004) and it was found here (1.6–120 ng/g sediment) and was indeed more abundant in the Group 3 sediments (Pan, 2015). Intriguingly, the samples with high MIs, RIs and GDGT-0/crenarchaeol ratios also contained abundant non-isoprenoidal dialkylglycerol ethers (DAGEs)

and *iso*/*anteiso*$C_{15:0}$ and *iso*/*anteiso*$C_{17:0}$ fatty acids (Pan, 2015), potentially derived from sulphate-reducing bacteria (Hinrichs et al., 2000; Pancost et al., 2001b). These could reflect independent bacterial inputs, or organisms syntrophically associated with archaeal methanotrophs. However, many thermophilic bacteria synthesize abundant DAGEs and *iso*- and *anteiso*-branched fatty acids (e.g. Huber et al., 1992; Sturt et al., 2004; Yang et al., 2006; Schubotz et al., 2013; Reeves et al., 2014). Moreover, many Archaea (including methanogens, halophiles, Marine Benthic Group B and Miscellaneous Crenarchaeotic Group) produce archaeol (e.g. Koga and Morii, 2005; Lipp and Hinrichs, 2009). In fact, many of these compounds have been detected in hydrothermal deposits that appear to have no AOM influence (e.g. Bradley et al., 2009; Kaur et al., 2011, 2015). As such, the co-occurrence of these biomarkers with high MIs could be evidence for an AOM influence, but that evidence is weak and other explanations remain possible. Compound-specific stable carbon isotope analysis could resolve these competing hypotheses (e.g. Pancost et al., 2001a; Elvert et al., 2005; Niemann and Elvert, 2008), but that was not possible due to their low abundances.

4.2. Isoprenoidal GMGTs

Isoprenoidal GMGTs were only found in some metalliferous sediments and low-temperature hydrothermal deposits from the SWIR, being absent in Group 1 sediments and occurring in relatively low abundances in Group 2 (mainly GMGT-0). Abundances were much higher in Group 3 (especially SW40 in M-T3, enriched in copper and zinc, and strongly influenced by high-temperature hydrothermal activity), and dominated by both GMGT-0 and GMGT-4.

GMGTs have been found in many marine sediments, albeit at generally low abundances

(Schouten et al., 2008); they appear to be particularly abundant in hydrothermal settings, including Loki's Castle (Jaeschke et al., 2012, 2014), Lost City (Lincoln et al., 2013; Méhay et al., 2013) and PACMANUS deep-sea hydrothermal fields (Reeves et al., 2014). They have been reported in *Methanobacteriales* (*Methanothermus fervidus*, Morii et al., 1998), *Thermococcales* (*T. celer*, *P. horikoshii*, Sugai et al., 2004; Jaeschke et al., 2012), DHVE2-cluster (*Aciduliprofundum boonei*, Reysenbach et al., 2006) and *Desulfurococcales* (*Ignisphaera aggregans*, Knappy et al., 2011). Because a thermophilic crenarchaeon and *Methanobacteriales* were previously detected in some of these samples (Peng et al., 2011; Li et al., 2013), we speculate that GMGTs (and maybe GTGT-0) in the metalliferous sediments and low-temperature hydrothermal deposits mainly originated from these archaea (Schouten et al., 2013b).

Additionally, there is a strong positive correlation between RI and percentages of GMGTs (of total tetraethers) in the metalliferous sediments strongly influenced by hydrothermal activity and low-temperature hydrothermal deposits from the SWIR (Fig. 6). A global synthesis shows that this correlation is generally widespread and somewhat consistent across a range of hydrothermal settings (Fig. 6; data from Jaeschke et al., 2012; Lincoln et al., 2013; Jaeschke et al., 2014; Reeves et al., 2014). Given the strong positive linear relationship between RI and temperature (Elling et al., 2015; Kaur et al., 2015), it seems likely temperature also governs the relative abundances of GMGTs – although again, we cannot entirely preclude a pH control. Regardless of the direct control, it seems clear that %GMGTs also are indicative of hydrothermal input in the SWIR, similar to what has been suggested for Lost City Hydrothermal Field (Lincoln et al., 2013).

4.3. Branched GDGTs of Putative Bacterial Origin

443 At the SWIR, proportions of *br*GDGTs are low (<10%) for most background sediments, M-
444 T1, M-T3 and some low-temperature hydrothermal deposits (mainly Group 1 and 3); similarly,
445 BIT indices were generally less than 0.10. These observations are consistent with those from
446 previous studies of open marine sediments, wherein *br*GDGT generally comprise less than 10%
447 of total GDGTs (Schouten et al., 2013b). Moreover, the low percentages of *br*GDGTs in M-T3,
448 which has been influenced by high-temperature hydrothermal activity, are similar to high-
449 temperature hydrothermal sulfides from other areas (Jaeschke et al., 2012; Reeves et al., 2014).
450 However, higher relative amounts of *br*GDGTs occurred in some background marine sediments
451 (e.g. SW12, SW21) of Group 1, the hydrothermally impacted metalliferous sediments (e.g.
452 SW32) and low-temperature hydrothermal deposits (e.g. SW33, SW36, SW41) of Group 2.
453 Distributions also differed, with GDGT-I being dominant over GDGT-III, GDGT-II and GDGT-
454 IIa in Group 1 and 3 but less so in Group 2; similarly, CBT and MBT indices were relatively
455 higher in Group 2 than in Group 1 and 3.
456 Although *br*GDGTs are mainly considered to be products of heterotrophic anaerobic
457 bacteria in terrigenous soil (Weijers et al., 2009), a thermophile source has been inferred for
458 some terrestrial hot springs (Hedlund et al., 2013; Zhang et al., 2013). Furthermore, it seems
459 likely that the terrigenous contribution to the organic matter in the study area, located at an ocean
460 ridge >2000 km away from the nearest mainland, was minor; this is consistent with minor inputs
461 of Al and Ti (terrigenous indicators) and very low abundances of leaf wax biomarkers (high-
462 molecular-weight fatty acids and alkanols, Pan, 2015). Instead, we suggest that the *br*GDGTs in
463 all samples but especially where proportions exceed 10% derive from in situ bacterial production;
464 this could include Acidobacteria which are abundant in some Group 2 samples (SW33 and SW36;
465 Li et al., 2013). Recent studies have shown that *br*GDGTs are synthesized by bacteria in marine

sediments (Peterse et al., 2009; Zhu et al., 2011), hydrothermal systems (Hu et al., 2012; Lincoln et al., 2013) and shelf systems (Sinninghe Damsté, 2016). However, it remains unclear why particularly high proportions are largely restricted to Group 2 sediments in this setting.

5. Synthesis

At submarine hydrothermal vents, microorganisms thrive on inorganic energy sources, such as methane, reduced iron and manganese that are abundant in hydrothermal vent fluids (Tagliabue et al., 2010; Breier et al., 2012). These inorganic elements are dispersed more widely by hydrothermal plumes rising hundreds of metres off the seafloor and traveling thousands of kilometres from the vents (Dick and Tebo, 2010; Toner et al., 2012; Fitzsimmons et al., 2014). The abundance of chemosynthetic microorganisms within hydrothermal plumes makes such plumes an important dispersal mechanism and a significant source of organic matter to the deep ocean (McCollum, 2000; Lam et al., 2004, 2008). Moreover, these microorganisms appear to be active in plumes and partially determine the geochemical fate of these hydrothermal inputs (Lilley et al., 1995).

Previous work has confirmed that species richness and phylogenetic diversity is typically highest near the vent orifice, with the abundance of chemosynthetic microorganisms decreasing with increasing distance from the vent (Sheik et al., 2015). This is consistent with our analyses. The M-T2 and M-T3 sites, with high Fe, Mn, Cu and Zn contents and in close proximity to the vent, have GDGT distributions similar to those of hydrothermal deposits and distinct from background sediments. Overall, the hydrothermal GDGT signature was consistent with previous work and the expected influence of higher growth temperature, including high Ring Indices, TEX_{86} values and %GMGT. Other features, including high %GDGT-0, appear to be consistent

with an active methane cycle in these sites. Crucially, the more distal M-T1 sediments have GDGT distributions largely indistinguishable from background sediments, suggesting a rapidly waning chemosynthetic contribution relative to normal marine contributions as the plume dispersed and was diluted.

Acknowledgements

We thank associate editor Dr. Ann Pearson and two anonymous reviewers for their comments that helped to improve an earlier version of this manuscript. We thank the staff in Organic Geochemistry Unit and the Bristol Node of the NERC Life Sciences Mass Spectrometry Facility for analytical support. We are also grateful to the participants in the cruise DY115-20 and 21 for collecting samples used in this research, and the crew members of R/V Da Yang Yihao. RDP thanks the RS Wolfson Research Merit Award. The study was supported by the Chinese National Key Basic Research Program (973 program, No. 2012CB417300), the National Natural Science Foundation of China (No.41376048), the Project of China Ocean Mineral Resources R & D Association (No.DY125-11-E-04/05).

References

Amon, D.J., Copley, J.T., Dahlgren, T.G., Horton, T., Kemp, K.M., Rogers, A.D., Glover, A.G., 2015. Observations of fauna attending wood and bone deployments from two seamounts on the Southwest Indian Ridge. Deep-Sea Research Part II: Topical Studies in Oceanography, http://dx.doi.org/10.1016/j.dsr2.2015.07.003.

Beaulieu, S.E., Baker, E.T., German, C.R., Maffei, A., 2013. An authoritative global database for active submarine hydrothermal vent fields. Geochemistry Geophysics Geosystems 14, 4892-

4905.

Blaga, C.I., Reichart, G.-J., Heiri, O., Sinninghe Damsté, J.S., 2009. Tetraether membrane lipid distributions in water-column particulate matter and sediments: a study of 47 European lakes along a north–south transect. Journal of Paleolimnology 41, 523-540.

Bligh, E., Dyer, W., 1959. A rapid method of total lipid extraction and purification. Canadian Journal of Biochemistry and Physiology 37, 911-917.

Blumenberg, M., Seifert, R., Reitner, J., Pape, T., Michaelis, W., 2004. Membrane lipid patterns typify distinct anaerobic methanotrophic consortia. Proceedings of the National Academy of Sciences of the United States of America 101: 11111-11116.

Blumenberg, M., Seifert, R., Buschmann, B., Kiel, S., Thiel, V., 2012. Biomarkers reveal diverse microbial communities in black smoker sulfides from Turtle Pits (Mid-Atlantic Ridge, Recent) and Yaman Kasy (Russia, Silurian). Geomicrobiology Journal 29, 66-75.

Boyd, E.S., Pearson, A., Pi, Y., Li, W.-J., Zhang,Y., He, L., Zhang, C.L., Geesey, G.G., 2011.Temperature and pH controls on glycerol dibiphytanyl glycerol tetraether lipid composition in the hyperthermophilic crenarchaeon Acidilobus sulfurireducens. Extremophiles 15, 59-65.

Boyd, E.S., Hamilton, T.L., Wang, J., He, L., Zhang, C.L., 2013. The role of tetraether lipid composition in the adaptation of thermophilic archaea to acidity. Frontiers in Microbiology 4, http://dx.doi.org/10.3389/fmicb.2013.00062.

Bradley, A.S., Fredricks, H., Hinrichs, K.-U, Summons, R.E., 2009. Structural diversity of diether lipids in carbonate chimneys at the Lost City Hydrothermal Field. Organic Geochemistry 40, 1169-1178.

Breier, J.A., Toner, B.M., Fakra, S.C., Marcus, M.A., White, S.N.,Thurnherr, A.M., German,

C.R., 2012. Sulfur, sulfides, oxides and organic matter aggregated in submarine hydrothermal plumes at 9°50′N East Pacific Rise. Geochimica et Cosmochimica Acta 88, 216-236.

Cao, Z., Cao, H., Tao, C., Li, J., Yu, Z., Shu, L., 2012. Rare earth element geochemistry of hydrothermal deposits from Southwest Indian Ridge. Acta Oceanologica Sinica 31, 62-69.

Chen C., Linse, K., Roterman, C.N., Copley, J.T., Rogers, A.D., 2015a. A new genus of large hydrothermal vent-endemic gastropod (Neomphalina: Peltospiridae). Zoological Journal of the Linnean Society 175, 319–335.

Chen, C., Copley, J.T., Linse, K., Rogers, A.D., Sigwart, J.D., 2015b.The heart of a dragon: 3D anatomical reconstruction of the 'scaly-foot gastropod' (Mollusca: Gastropoda: Neomphalina) reveals its extraordinary circulatory system. Frontiers in Zoology, http://dx.doi.org/10.1186/s12983-015-0105-1.

Chen C., Linse, K., Copley, J.T., Rogers, A.D., 2015c. The 'scaly-foot gastropod': a new genus and species of hydrothermal vent-endemic gastropod (Neomphalina: Peltospiridae) from the Indian Ocean. Journal of Molluscan Studies, http://dx.doi.org/10.1093/mollus/eyv013.

Chen C., Copley, J.T., Linse, K., Rogers, A.D., 2015d. Low connectivity between 'scaly-foot gastropod' (Mollusca: Peltospiridae) populations at hydrothermal vents on the Southwest Indian Ridge and the Central Indian Ridge. Organisms Diversity & Evolution 15, 663-670.

Chowdhury, T.R., Dick, R.P., 2012. Standardizing methylation method during phospholid fatty acid analysis to profile soil microbial communities. Journal of Microbiological Methods 88, 285-291.

Cole, C., Coelho, A.V., James, R.H., Connelly, D., Sheehan, D., 2014. Proteomic responses to metal-induced oxidative stress in hydrothermal vent-living mussels, Bathymodiolus sp., on

the Southwest Indian Ridge. Marine Environmental Research 96, 29-37.

Copley, J.T., 2011. Research cruise JC67, Dragon vent field, SW Indian Ocean, 27–30 November 2011. In: RRS James Cook cruise report. British Oceanographic Data Centre. Available from http://www.bodc.ac.uk/data/information_and_inventories/cruise_inventory/report /10593/ (last accessed 1 March 2016).

Corliss, J.B., Dymond, J., Gordon, L.I., Edmond, J.M., von Herzen, R.P., Ballard, R.D., Green, K., Williams, D., Bainbridge, A., Crane, K., van Andel, T.H., 1979. Submarine thermal springs on the Galapagos Rift. Science 203, 1073-1083.

Dias, A., Mills, R., Taylor, R., Ferreira, P., Barriga, F., 2008. Geochemistry of a sediment push-core from the Lucky Strike hydrothermal field, Mid-Atlantic Ridge. Chemical Geology 247, 339-351.

Dick, G.J., Tebo, B.M., 2010. Microbial diversity and biogeochemistry of the Guaymas Basin deep-sea hydrothermal plume. Environmental Microbiology 12, 1334-1347.

Dickson, L., Bull, I.D., Gates, P.J., Evershed, R.P., 2009. A simple modification of a silicic acid lipid fractionation protocol to eliminate free fatty acids from glycolipid and phospholipid fractions. Journal of Microbiological Methods 78, 249-254.

Ding, K., Seyfried Jr., W.E., Zhang, Z., Tivey, M.K., Von Damm, K.L., Bradley, A.M., 2005. The in situ pH of hydrothermal fluids at mid-ocean ridges. Earth and Planetary Science Letters 237, 167-174.

Douville, E., Charlou, J.L., Oelkers, E.H., Bienvenu, P., Jove Colon, C.F., Donval, J.P., Fouquet, Y., Prieur, D., Appriou, P., 2002. The rainbow vent fluids (36°14’N, MAR): The influence of ultramafic rocks and phase separation on trace metal content in Mid-Atlantic Ridge hydrothermal fluids. Chemical Geology 184, 37-48.

581 Elling, F.J., Könneke, M., Mußmann, M., Greve, A., Hinrichs, K.-U., 2015. Influence of
582 temperature, pH, and salinity on membrane lipid composition and TEX_{86} of marine
583 planktonic thaumarchaeal isolates. Geochimica et Cosmochimica Acta 171, 238-255.
584 Elvert, M., Hopmans, E.C., Treude, T., Boetius, A., Suess, E., 2005. Spatial variations of
585 methanotrophic consortia at cold methane seeps: implications from a high-resolution
586 molecular and isotopic approach. Geobiology 3, 195-209.
587 Fitzsimmons, J.N., Boyle, E.A., Jenkins, W.J., 2014. Distal transport of dissolved hydrothermal
588 iron in the deep South Pacific Ocean. Proceedings of the National Academy of Sciences 111,
589 16654-16661.
590 Fontugne, M.R., Jouanneau, J.M., 1987. Modulation of the particulate organic carbon flux to the
591 ocean by a macrotidal estuary evidence from measurements of carbon isotopes in organic
592 matter from the Gironde system. Estuarine, Coastal and Shelf Science 24, 377-387.
593 Froneman, P.W., Pakhomov, E.A., Perissinotto, R., Meaton, V., 1998. Feeding and predation
594 impact of two chaetognath species, Eukrohnia hamata and Sagitta gazellae, in the vicinity of
595 Marion Island (Southern ocean). Marine Biology 131, 95-101.
596 German, C.R., Baker, E.T., Mevel, C., Tamaki, K., the FUJI Science Team, 1998. Hydrothermal
597 activity along the southwest indian ridge. Nature 395, 490-493.
598 Gibson, R.A., van der Meer, M.T., Hopmans, E.C., Reysenbach, A.L., Schouten, S., Sinninghe
599 Damsté, J.S., 2013. Comparison of intact polar lipid with microbial community composition
600 of vent deposits of the Rainbow and Lucky Strike hydrothermal fields. Geobiology 11, 72-85.
601 Govenar, B., 2012. Energy transfer through food webs at hydrothermal vents: Linking the
602 lithosphere to the biosphere. Oceanography 25, 246-255.
603 Hatta, M., Measures, C.I., Wu, J., Roshan, S., Fitzsimmons, J.N., Sedwick, P., Morton, P., 2015.

An overview of dissolved Fe and Mn distributions during the 2010–2011 U.S. GEOTRACES north Atlantic cruises: GEOTRACES GA03. Deep-Sea Research Part II: Topical Studies in Oceanography 116, 117-129.

Hedlund B.P., Paraiso, J.J., Williams, A.J., Huang, Q., Wei, Y., Dijkstra, P., Hungate, B.A., Dong, H., Zhang, C.L., 2013. Wide distribution of autochthonous branched glycerol dialkyl glycerol tetraethers (bGDGTs) in U.S. Great Basin hot springs. Frontiers in Microbiology 4, http://dx.doi.org/10.3389/fmicb.2013.00222.

Hinrichs, K.-U., Summons, R.E., Orphan, V.J., Sylva, S.P., Hayes, J.M., 2000. Molecular and isotopic analysis of anaerobic methane-oxidizing communities in marine sediments. Organic Geochemistry 31, 1685-1701.

Hopmans, E.C., Schouten, S., Pancost, R.D., van der Meer, M.T.J., Sinninghe Damsté, J.S., 2000. Analysis of intact tetraether lipids in archaeal cell material and sediments by high performance liquid chromatography atmospheri pressure chemical ionization mass spectrometry. Rapid Communications in Mass Spectrometry 14, 585-589.

Hopmans, E.C., Weijers, J.W.H., Schefuβ, E., Herfort, L., Sinninghe Damsté, J.S., 2004. A novel proxy for terrestrial organic matter in sediments based on branched and isoprenoid tetraether lipids. Earth and Planetary Science Letters 225, 107-116.

Hu, J., Meyers, P.A., Chen, G., Peng, P., Yang, Q., 2012. Archaeal and bacterial glycerol dialkyl glycerol tetraethers in sediments from the Eastern Lau Spreading Center, South Pacific Ocean. Organic Geochemistry 43, 162-167.

Huang, X., Zeng, Z., Chen, S., Yin, X., Wang, X., Zhao, H., Yang, B., Rong, K., Ma, Y., 2014. Component characteristics of organic matter in hydrothermal barnacle shells from Southwest Indian Ridge. Acta Oceanologica Sinica 32, 60-67.

627 Huber, R., Wilharm, T., Huber, D., Trincone, A., Burggraf, S., König, H., Reinhard, R.,
628 Rockinger, I., Fricke, H., Stetter, K.O., 1992. *Aquifex pyrophilus* gen. Nov. sp. nov.,
629 represents a novel group of marine hyperthermophilic hydrogen-oxidizing bacteria.
630 Systematic Applied Microbiology 15, 340-351.
631 Huguet, C., Hopmans, E.C., Febo-Ayala, W., Thompson, D.H., Sinninghe Damsté, J.S., Schouten,
632 S., 2006. An improved method to determine the absolute abundance of glycerol dibiphytanyl
633 glycerol tetraether lipids. Organic Geochemistry 37, 1036-1041.
634 Jaeschke, A., Jørgensen, S.L., Bernasconi, S.M., Pedersen, R.B., Thorseth, I.H., Früh-Green, G.L.,
635 2012. Microbial diversity of Loki's Castle black smokers at the Arctic Mid-Ocean Ridge.
636 Geobiology 10, 548-561.
637 Jaeschke, A., Eickmann, B., Lang, S.Q., Bernasconi, S.M., Strauss, H., Früh-Green, G.L., 2014.
638 Biosignatures in chimney structures and sediment from the Loki's Castle low-temperature
639 hydrothermal vent field at the Arctic Mid-Ocean Ridge. Extremophiles 18, 545-560.
640 Kashefi, K., Lovley, D.R., 2003. Extending the Upper Temperature Limit for life. Science 301,
641 934.
642 Kato, S., Takano, Y., Kakegawa, T., Oba, H., Inoue, K., Kobavashi, C., Utsumi, M., Marumo, K.,
643 Kobavashi, K., Ito,Y., Ishibashi, J., Yamagishi, A., 2010. Biogeography and biodiversity in
644 sulfide structures of active and inactive vents at deep-sea hydrothermal fields of Southern
645 Mariana Trough. Applied and Environmental Microbiology 76, 2968-2979.
646 Kaur, G., Mountain, B.W., Hopmans, E.C., Pancost, R.D., 2011. Relationship between lipid
647 distribution and geochemical environment within Champagne Pool, Waiotapu, New Zealand.
648 Organic Geochemistry 42, 1203-1215.
649 Kaur, G., Mountain, B.W., Stott, M.B., Hopmans, E.C., Pancost, R.D., 2015. Temperature and pH

control on lipid composition of silica sinters from diverse hot springs in the Taupo Volcanic Zone, New Zealand. Extremophiles 19, 327-344.

Kellermann, M.Y., Wegener, G., Elvert, M., Yoshinaga, M.Y., Lin, Y.-S., Holler, T., Mollar, X.P., Knittel, K., Hinrichs, K.-U., 2012. Autotrophy as a predominant mode of carbon fixation in anaerobic methane-oxidizing microbial communities. Proceedings of the National Academy of Sciences 109, 19321-19326.

Kim, J., Schouten, S., Hopmans, E.C., Donner, B., Sinninghe Damsté, J.S., 2008. Global sediment core-top calibration of the TEX86 paleothermometer in the ocean. Geochimica et Cosmochimica Acta 72, 1154-1173.

Kim, J.-H., van der Meer, J., Schouten, S., Helmke, P., Willmott, V., Sangiorgi, F., Koç, N., Hopmans, E.C., Sinninghe Damsté, J.S., 2010. New indices and calibrations derived from the distribution of crenarchaeal isoprenoid tetraether lipids: implications for past sea surface temperature reconstructions. Geochimica et Cosmochimica Acta 74, 4639-4654.

Klunder, M.B., Laan, P., Middag, R., De Baar, H.J.W., van Ooijen, J.C., 2011. Dissolved iron in the Southern Ocean (Atlantic sector). Deep-Sea Research Part II: Topical Studies in Oceanography 58, 2678-2694.

Knappy, C.S., Nunn, C.E., Morgan, H.W., Keely, B.J., 2011. The major lipid cores of the archaeon Ignisphaera aggregans: implications for the phylogeny and biosynthesis of glycerol monoalkyl glycerol tetraether isoprenoid lipids. Extremophiles 15, 517-528.

Koga, Y., Morii, H., 2005. Recent advances in structural research on ether lipids from archaea including comparative and physiological aspects. Bioscience Biotechnology and Biochemistry 69, 2019-2034.

Kormas, K.A., Tivey, M.K., Von Damm, K., Teske, A., 2006. Bacterial and archaeal phylotypes

673 associated with distinct mineralogical layers of a white smoker spire from a deep-sea
674 hydrothermal vent site (9°N, East Pacific Rise). Environmental Microbiology 8, 909-920.
675 Lam, P., Cowen, J.P., Jones, R.D., 2004. Autotrophic ammonia oxidation in a deep-sea
676 hydrothermal plume. FEMS Microbiology Ecology 47, 191-206.
677 Lam, P., Cowen, J.P., Popp, B.N., Jones, R.D., 2008. Microbial ammonia oxidation and enhanced
678 nitrogen cycling in the Endeavour hydrothermal plume. Geochimica et Cosmochimica Acta
679 72, 2268-2286.
680 Lei, J., Chu, F., Yu, X., Li, X., Tao, C., Ge, Q., 2015. Composition and genesis implications of
681 hydrocarbons in 49.6°E hydrothermal area, Southwest Indian Ocean Ridge. Earth Science
682 Frontiers 22, 281-290.
683 Lengger, S.K., Hopmans, E.C., Sinninghe Damsté, J.S., Schouten, S., 2012. Comparison of
684 extraction and work up techniques for analysis of core and intact polar tetraether lipids from
685 sedimentary environments. Organic Geochemistry 47, 34-40.
686 Li, J., Peng, X., Zhou, H., Li, J., Sun, Z., 2013. Molecular evidence for microorganisms
687 participating in Fe, Mn, and S biogeochemical cycling in two low-temperature hydrothermal
688 fields at the Southwest Indian Ridge. Journal of Geophysical Research: Biogeosciences 118,
689 665-679.
690 Li, J., Zhou, H., Fang, J., Wu, Z., Peng, X., 2015. Microbial Distribution in a Hydrothermal
691 Plume of the Southwest Indian Ridge. Geomicrobiology Journal,
692 http://dx.doi.org/10.1080/01490451.2015.1048393.
693 Lilley, M.D., Feely, R.A., Trefry, J.H., 1995. Chemical and biochemical transformations in
694 hydrothermal plumes. In *Seafloor Hydrothermal Systems: Physical, Chemical, Biological,*
695 *and Geological Interactions*. Humphris, S.E., Zierenberg, R.A., Mullineaux, L.S., and

696 Thomson, R.E.(eds). Washington, DC, USA: American Geophysical Union, pp. 369-391.
697 Lincoln, S.A., Bradley, A.S., Newman, S.A., Summons, R.E., 2013. Archaeal and bacterial
698 glycerol dialkyl glycerol tetraether lipids in chimneys of the Lost City Hydrothermal Field.
699 Organic Geochemistry 60, 45-53.
700 Lipp, J.S., Hinrichs, K.-U., 2009. Structural diversity and fate of intact polar lipids in marine
701 sediments. Geochimica et Cosmochimica Acta 73, 6816-6833.
702 Llido, J., Garçon, V., Lutjeharms, J., Sudre, J., 2005. Event-scale blooms drive enhanced primary
703 productivity at the Subtropical Convergence. Geophysical Research Letters, 32-L15611.
704 Méhay, S., Früh-Green, G.L., Lang, S.Q., Bernasconi, S.M., Brazelton, W.J., Schrenk, M.O.,
705 Schaeffer, P., Adam, P., 2013. Record of archaeal activity at the serpentinite-hosted Lost City
706 Hydrothermal Field. Geobiology 11, 570-592.
707 McCollom, T.M., 2000. Geochemical constraints on primary productivity in submarine
708 hydrothermal vent plumes. Deep Sea Research Part I: Oceanographic Research Papers 47,
709 85-101.
710 McCollom, T.M., Seewald, J.S., German, C.R., 2015. Investigation of extractable organic
711 compounds in deep-sea hydrothermal vent fluids along the Mid-Atlantic Ridge. Geochimica
712 et Cosmochimica Acta 156, 122-144.
713 Morii, H., Eguchi, T., Nishihara, M., Kakinuma, K., König, H., Koga, Y., 1998. A novel ether
714 core lipid with H-shaped C 80-isoprenoid hydrocarbon chain from the hyperthermophilic
715 methanogen Methanothermus fervidus. Biochimica et Biophysica Acta (BBA)-Lipids and
716 Lipid Metabolism 1390, 339-345.
717 Mrozik, A., Nowak, A., Piotrowska-Seget, Z., 2014. Microbial diversity in waters, sediments and
718 microbial mats evaluated using fatty acid-based methods. International Journal of

719 Environmental Science and Technology 11, 1487-1496.
720 Niemann, H., Elvert, M., 2008. Diagnostic lipid biomarker and stable carbon isotope signatures
721 of microbial communities mediating the anaerobic oxidation of methane with sulphate.
722 Organic Geochemistry 39, 1668-1677.
723 Noble, A.E., Lamborg, C.H., Ohnemus, D.C., Lam, P.J., Goepfert, T.J., Measures, C.I., Frame,
724 C.H., Casciotti, K.L., DiTullio, G.R., Jennings, J.C., Saito, M.A., 2012. Basin-scale inputs of
725 cobalt, iron, and manganese from the Benguela-Angola front to the South Atlantic Ocean.
726 Limnology and Oceanography 57, 989-1010.
727 Oba, M., Sakata, S., Tsunogai, U., 2006. Polar and neutral isopranyl glycerol ether lipid as
728 biomarkers of archaea in near-surface sediments from the Nankai Trough. Organic
729 Geochemistry 37, 1643-1654.
730 Pan, A., 2015. Research on characteristics of lipid biomarkers in the subseafloor hydrothermal
731 environments and terrestrial hot springs. PhD dissertation of Tongji University.
732 Pancost, R.D., Hopmans, E.C., Sinninghe Damsté, J.S., Medinauth Scientific Party, 2001a.
733 Archaeal lipids in Mediterranean cold seeps: molecular proxies for anaerobic methane
734 oxidation. Geochimica et Cosmochimica Acta 65, 1611-1627.
735 Pancost, R.D., Bouloubassi, I., Aloisi, G., Sinninghe Damsté, J.S., Medinauth Scientific Party,
736 2001b. Three series of non-isoprenoidal dialkyl glycerol diethers in cold-seep carbonate
737 crusts. Organic Geochemistry 32, 695-707.
738 Pancost, R.D., Pressley, S., Coleman, J.M., Benning, L.G., Mountain, B.W., 2005. Lipid
739 biomolecules in silica sinters: indicators of microbial biodiversity. Environmental
740 Microbiology 7, 66-77.
741 Pancost, R.D., Pressley, S., Coleman, J.M., Talbot, H.M., Kelly, S.P., Farrimond, P., Schouten, S.,

742 Benning, L.G., Mountain, B.W., 2006. Composition and implications of diverse lipids in
743 New Zealand Geothermal sinters. Geobiology 4, 71-92.
744 Pearson, A., Huang, Z., Ingalls, A., Romanek, C., Wiegel, J., Freeman, K., Smittenberg, R.,
745 Zhang, C., 2004. Nonmarine crenarchaeol in Nevada hot springs. Applied and
746 Environmental Microbiology 70, 5229-5237.
747 Pearson, A., Pi, Y., Zhao, W., Li, W., Li, Y., Inskeep, W., Perevalova, A., Romanek, C., Li, S.,
748 Zhang, C.L., 2008. Factors controlling the distribution of archaeal tetraethers in terrestrial
749 hot springs. Applied and Environmental Microbiology 74, 3523-3532.
750 Pearson, A., Ingalls, A., 2013. Assessing the use of archaeal lipids as marine environmental
751 proxies. Annual Review of Earth and Planetary Sciences 41, 359-384.
752 Peng, X., Chen, S., Zhou, H., Zhang, L., Wu, Z., Li, J., Li, J., Xu, H., 2011. Diversity of biogenic
753 minerals in low-temperature Si-rich deposits from a newly discovered hydrothermal field on
754 the ultraslow spreading Southwest Indian Ridge. Journal of Geophysical Research 116,
755 G03030. http://dx.doi.org/10.1029/2011JG001691.
756 Peterse, F., Kim, J.-H., Schouten, S., Kristensen, D.K., Koç, N., Sinninghe Damsté, J.S., 2009.
757 Constraints on the application of the MBT/CBT palaeothermometer at high latitude
758 environments (Svalbard, Norway). Organic Geochemistry 40, 692-699.
759 Phleger, C.F., Nelson, M.M., Groce, A.K., Cary, S.C., Coyne, K.J., Nichols, P.D., 2005. Lipid
760 composition of deep-sea hydrothermal vent tubeworm Riftia pachyptila, crabs Munidopsis
761 subsquamosa and Bythograea thermydron, mussels Bathymodiolus sp. and limpets
762 Lepetodrilus spp. Comparative Biochemistry and Physiology Part B: Biochemistry and
763 Molecular Biology 141, 196-210.
764 Pitcher, A., Hopmans, E.C., Schouten, S., Sinninghe Damsté, J.S., 2009. Separation of core and

765 intact polar archaeal tetraether lipids using silica columns: Insights into living and fossil
766 biomass contributions. Organic Geochemistry 40, 12-19.
767 Pitcher, A., Hopmans, E.C., Mosier, A.C., Park, S.-J., Rhee, S.-K., Francis, C.A., Schouten, S.,
768 Sinninghe Damsté, J.S., 2011. Core and intact polar glycerol dibiphytanyl glycerol tetraether
769 lipids of ammonia-oxidizing archaea enriched from marine and estuarine sediments. Applied
770 and Environmental Microbiology 77, 3468-3477.
771 Premuzic, E., Benkovitz, C.M., Gaffney, J., Walsh, J., 1982. The nature and distribution of
772 organic matter in the surface sediments of world oceans and seas. Organic Geochemistry 4,
773 63-72.
774 Reeves, E.P., Yoshinaga, M.Y., Pjevac, P., Goldenstein, N.I., Peplies, J., Meyerdierks, A., Amann,
775 R., Bach, W., Hinrichs, K.-U., 2014. Microbial lipids reveal carbon assimilation patterns on
776 hydrothermal sulfide chimneys. Environmental Microbiology 16, 3515-3532.
777 Reysenbach, A.-L., Liu, Y., Banta, A.B., Beveridge, T.J., Kirshtein, J.D., Schouten, S., Tivey,
778 M.K., Von Damm, K.L., Voytek, M.A., 2006. A ubiquitous thermoacidophilic archaeon from
779 deep-sea hydrothermal vents. Nature 442, 444-447.
780 Rogers, A.D., Boersch-Supan, P.H., Chen, C., Chivers, A., Copley, J.T., Djurhuus, A., Ferrero,
781 T.J., Huhnerbach, V., Lamont, P., Marsh, L., Muller, E., Packer, M., Read, J.F., Serpetti, N.,
782 Shale, D., Staples, D., Taylor, M.A., Webster, C., Woodall, L., 2012. Benthic Biodiversity of
783 Seamounts in the southwest Indian Ocean. Cruise Report “RRS James Cook” Southern
784 Indian Ocean Seamounts (IUCN/UNDP/ASCLME/ NERC Cruise 66) 7th November–21st
785 December.
786 Schouten, S., Hopmans, E.C., Schefuβ, E., Sinninghe Damsté, J.S., 2002. Distributional
787 variations in marine crenarchaeotal membrane lipids: a new organic proxy for reconstructing

788 ancient sea water temperatures?. Earth and Planetary Science Letters 204, 265-274.
789 Schouten, S., Wakeham, S.G., Hopmans, E.C., Sinninghe Damsté, J.S., 2003. Biogeochemical
790 evidence that thermophilic archaea mediate the anaerobic oxidation of methane. Applied and
791 Environmental Microbiology 69, 1680-1686.
792 Schouten, S., Huguet, C., Hopmans, E.C., Kienhuis, M.V.M., Sinninghe Damsté, J.S., 2007a.
793 Analytical methodology for TEX86 paleothermometry by high performance liquid
794 chromatography/atmospheric pressure chemical ionization-mass spectrometry. Analytical
795 Chemistry 79, 2940-2943.
796 Schouten, S., van der Meer, M.T., Hopmans, E.C., Rijpstra, W.I., Reysenbach, A.L., Ward, D.M.,
797 Sinninghe Damsté, J.S., 2007b. Archaeal and bacterial glycerol dialkyl glycerol tetraether
798 lipids in hot springs of yellowstone national park. Applied Environmental Microbiology 73,
799 6181-6191.
800 Schouten, S., Baas, M., Hopmans, E.C., Sinninghe Damsté, J.S., 2008. An unusual isoprenoid
801 tetraether lipid in marine and lacustrine sediments. Organic Geochemistry 39, 1033-1038.
802 Schouten, S., Hopmans, E.C., van der Meer, J., Mets, A., Bard, E., Bianchi, T.S., Diefendorf, A.,
803 Escala, M., Freeman, K.H., Furukawa, Y., Huguet, C., Ingalls, A., Ménot-Combes, G.,
804 Nederbragt, A.J., Oba, M., Pearson, A., Pearson, E.J., RosellMelé, A., Schaeffer, P., Shah,
805 S.R., Shanahan, T.M., Smith, R.W., Smittenberg, R., Talbot, H.M., Uchida, M., Van Mooy,
806 B.A.S., Yamamoto, M., Zhang, Z., Sinninghe Damsté, J.S., 2009. An interlaboratory study of
807 TEX86 and BIT analysis using high-performance liquid chromatography mass spectrometry.
808 Geochemistry Geophysics Geosystems 10, Q03012, doi:10.1029/2008GC002221.
809 Schouten, S., Hopmans, E.C., Rosell- Melé, A., Pearson, A., Adam, P., Bauersachs, T., Bard, E.,
810 Bernasconi, S.M., Bianchi, T.S., Brocks, J.J., Carlson, L.T., Castañeda, I.S., Derenne, S.,

811 Doğrul Selver, A., Dutta, K., Eglinton, T., Fosse, C., Galy, V., Grice, K., Hinrichs, K.-U.,
812 Huang, Y., Huguet, A., Huguet, C., Hurley, S., Ingalls, A., Jia, G., Keely, B., Knappy, C.,
813 Kondo, M., Krishnan, S., Lincoln, S., Lipp, J., Mangelsdorf, K., Martínez-García, A., Ménot,
814 G., Mets, A., Mollenhauer, G., Ohkouchi, N., Ossebaar, J., Pagani, M., Pancost, R.D.,
815 Pearson, E.J., Peterse, F., Reichart, G.-J., Schaeffer, P., Schmitt, G., Schwark, L., Shah, S.R.,
816 Smith, R.W., Smittenberg, R.H., Summons, R.E., Takano, Y., Talbot, H.M., Taylor, K.W.R.,
817 Tarozo, R., Uchida, M., van Dongen, B.E., Van Mooy, B.A.S., Warren, C., Weijers, J.W.H.,
818 Werne, J.P., Woltering, M., Xie, S., Yamamoto, M., Yang, H., Zhang, C., Zhang, Y., Zhao, M.,
819 Sinninghe Damsté., 2013a. An interlaboratory study of TEX_{86} and BIT analysis of sediments,
820 extracts, and standard mixtures. Geochemistry Geophysics Geosystems 14, 5263-5285.
821 Schouten, S., Hopmans, E.C., Sinninghe Damsté, J.S., 2013b. The organic geochemistry of
822 glycerol dialkyl glycerol tetraether lipids: A review. Organic Geochemistry 54, 19-61.
823 Schubotz, F., Meyer-Dombard, D.R., Bradley, A.S., Fredricks, H.F., Hinrichs, K.-U., Shock, E.L.,
824 Summons, R.E., 2013. Spatial and temporal variability of biomarkers and microbial diversity
825 reveal metabolic and community flexibility in Streamer Biofilm Communities in the Lower
826 Geyser Basin, Yellowstone National Park. Geobiology 11, 549-569.
827 Sheik, C.S., Anantharaman, K., Breier, J.A., Sylvan, J.B., Edwards, K.J., Dick, G., 2015.
828 Spatially resolved sampling reveals dynamic microbial communities in rising hydrothermal
829 plumes across a back-arc basin. International Society for Microbial Ecology Journal 9, 1434-
830 1445.
831 Sinninghe Damsté, 2016. Spatial heterogeneity of sources of branched tetraethers in shelf
832 systems: The geochemistry of tetraethers in the Berau River delta (Kalimantan, Indonesia).
833 Geochimica et Cosmochimica Acta 186, 13-31.

834 Sogin, M.L., Morrison, H.G., Huber, J.A., Mark Welch, D., Huse, S.M., Neal, P.R., Arrieta, J.M.,
835 Herndl, G.J., 2006. Microbial diversity in the deep sea and the underexplored “rare
836 biosphere”. Proceedings of the National Academy of Science of the United States of
837 America 103, 12115-12120.
838 Sturt, H.F., Summons, R.E., Smith, K., Elvert M., Hinrichs, K.-U., 2004. Intact polar membrane
839 lipids in prokaryotes and sediments deciphered by high-performance liquid chromatography/
840 electrospray ionization multistage mass spectrometry – new biomarkers for biogeochemistry
841 and microbial ecology. Rapid Communications in Mass Spectrometry 18, 617-628.
842 Sugai, A., Uda, I., Itoh, Y.H., Itoh, T., 2004. The core lipid composition of the 17 strains of
843 hyperthermophilic archaea, Thermococcales. Journal of Oleo Science 53, 41-44.
844 Tagliabue, A., Bopp, L., Dutay, J.-C., Bowie, A.R., Chever, F., Jean-Baptiste, P., Bucciarelli, E.,
845 Lannuzel, D., Remenyi, T., Sarthou, G., Aumont, O., Gehlen, M., Jeandel, C., 2010.
846 Hydrothermal contribution to the oceanic dissolved iron inventory. Nature Geoscience 3,
847 252-256.
848 Takai, K., Komatsu, T., Inagaki, F., Horikoshi, K., 2001. Distribution of archaea in a black
849 smoker chimney structure. Applied and Environmental Microbiology 67, 3618-3629.
850 Tao, C., Lin, J., Guo, S., Chen, Y., Wu, G., Han, X., German, C., Yoerger, D., Zhu, J., Zhou, N.,
851 2007. The Chinese DY115-19 Cruise: Discovery of the first active hydrothermal vent field at
852 the ultraslow spreading Southwest Indian Ridge. InterRidge News 16, 25-26.
853 Tao, C., Li, H., Huang, W., Han, X., Wu, G., Su, X., Zhou, N., Lin, J., He, Y., Zhou, J., 2011.
854 Mineralogical and geochemical features of sulfide chimneys from the 49°39′ E hydrothermal
855 field on the Southwest Indian Ridge and their geological inferences. Chinese Science
856 Bulletin 56, 2828-2838.

857 Tao, C., Lin, J., Guo, S., Chen, Y.J., Wu, G., Han, X., German, C.R., Yoerger, D.R., Zhou, N., Li,
858 H., Su, X., Zhu, J., 2012. First active hydrothermal vents on an ultraslow-spreading center:
859 Southwest Indian Ridge. Geology 40, 47-50.
860 Toner, B., Marcus, M., Edwards, K., Rouxel, O., German, C., 2012. Measuring the form of iron
861 in hydrothermal plume particles. Oceanography 25, 209-212.
862 Uda, I., Sugai, A., Itoh, Y.H., Itoh, T., 2004. Variation in molecular species of core lipids from the
863 order Thermoplasmales strains depends on the growth temperature. Journal of Oleo Science
864 53, 399-404.
865 Villanueva, L., Sinninghe Damsté, J.S., Schouten, S., 2014. A re-evaluation of the archaeal
866 membrane lipid biosynthetic pathway. Nature Reviews Microbiology 12, 438-448.
867 Von Damm, K.L., Edmond, J.M., Grant, B., Measures, C.I., Walden, B., Weiss, R.F., 1985.
868 Chemistry of submarine hydrothermal solutions at 21°N, East Pacific Rise. Geochimica et
869 Cosmochimica Acta 49, 2197-2220.
870 Wang, H., Zhou, H., Yang, Q., Lilley, M.D., Wu, J., Ji, F., 2015. Development and application of
871 a gas chromatography method for simultaneously measuring H_2 and CH_4 in hydrothermal
872 plume samples. Limnology and Oceanography: Methods 13, 722-730.
873 Weijers, J.W.H., Schouten, S., van Den Donker, J.C., Hopmans, E.C., Sinninghe Damsté, J.S.,
874 2007. Environmental controls on bacterial tetraether membrane lipid distribution in soils.
875 Geochimica et Cosmochimica Acta 71, 703-713.
876 Weijers, J.W.H., Panoto, E., van Bleijswijk, J., Schouten, S., Rijpstra, W.I.C., Balk, M., Stams,
877 A.J.M., Sinninghe Damsté, J.S., 2009. Constraints on the biological source(s) of the orphan
878 branched tetraether membrane lipids. Geomicrobiology Journal 26, 402-414.
879 Wu, W., Zhang, C.L., Wang, H., He, L., Li, W., Dong, H., 2013. Impacts of temperature and pH

on the distribution of archaeal lipids in Yunnan hot springs, China. Frontiers in Microbiology 4, http://dx.doi.org/10.3389/fmicb.2013.00312.

Yang, Y.-L., Yang, F.-L., Jao, S.-C., Chen, M.-Y., Tsay, S.-S., Zou, W., Wu, S.-H., 2006. Structural elucidation of phosphoglycolipids from strains of the bacterial thermophiles *Thermus* and *Meiothermus*. Journal of Lipid Research 47, 1823-1832.

Zhang, Y.G., Zhang, C.L., Liu, X.-L., Li, L., Hinrichs, K.-U., Noakes, J.E., 2011. Methane Index: A tetraether archaeal lipid biomarker indicator for detecting the instability of marine gas hydrates. Earth and Planetary Science Letters 307, 525-534.

Zhang C.L., Wang, J., Dodsworth, J.A., Williams, A.J., Zhu, C., Hinrichs, K.-U, Zheng, F., Hedlund, B.P., 2013. In situ production of branched glycerol dialkyl glycerol tetraethers in a great basin hot spring (USA). Frontiers in Microbiology 4, http://dx.doi.org/ 10.3389/fmicb.2013.00181.

Zhou, H., Dick, H.J.B., 2013. Thin crust as evidence for depleted mantle supporting the Marion Rise. Nature 494, 195-200.

Zhu, C., Weijers, J.W.H., Wagner, T., Pan, J.M., Chen, J.F., Pancost, R.D., 2011. Sources and distributions of tetraether lipids in surface sediments across a large river-dominated continental margin. Organic Geochemistry 42, 376-386.

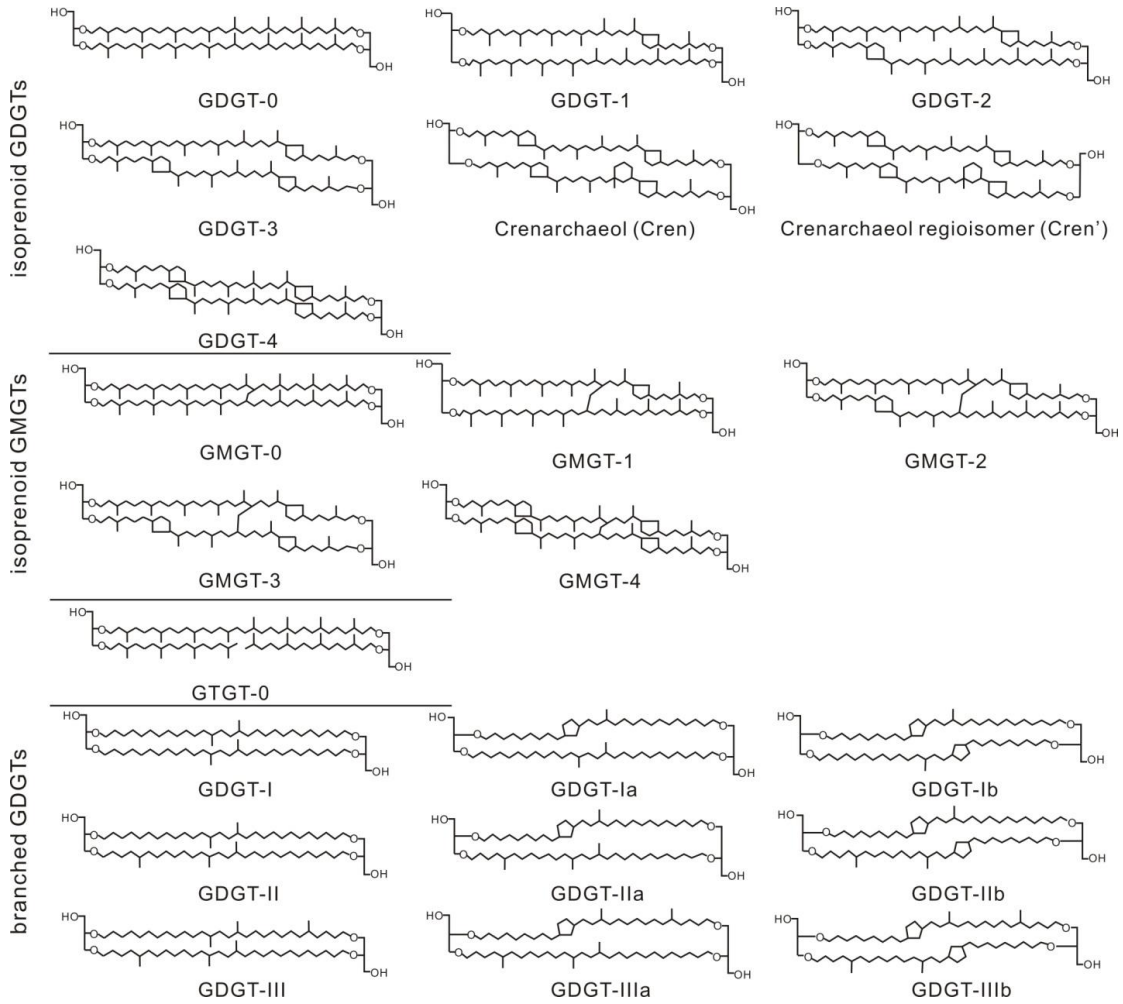

Fig. 1. Structures of tetraether lipids detected in SWIR hydrothermal field.

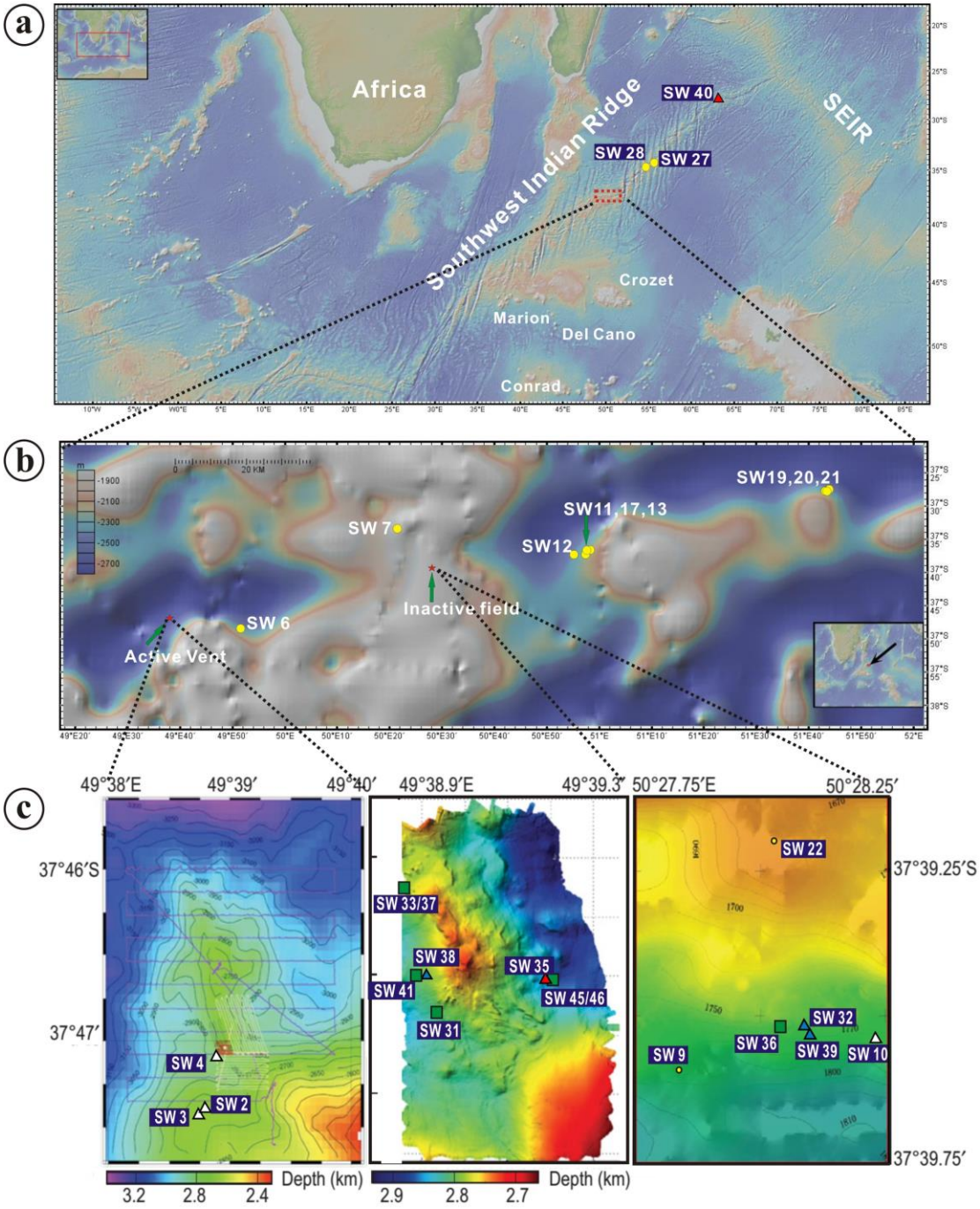

Fig. 2. Location of the samples collected from SWIR. Yellow circles mark background sediments; white, blue and red triangles mark M-T1, M-T2 and M-T3, respectively; green squares mark low-temperature hydrothermal deposits. Panel c modified after (Tao et al., 2012).

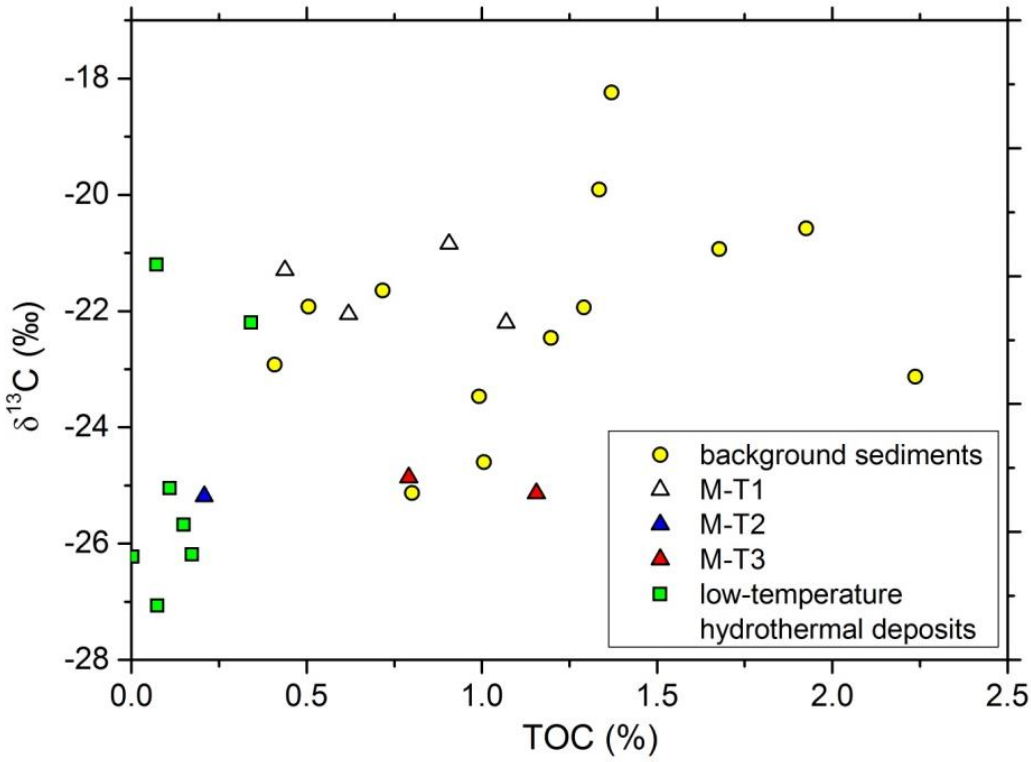

Fig. 3. Crossplot showing the overall positive correlation between TOC content and $\delta^{13}C_{TOC}$ values in background and metalliferous sediments and hydrothermal deposits from the SWIR.

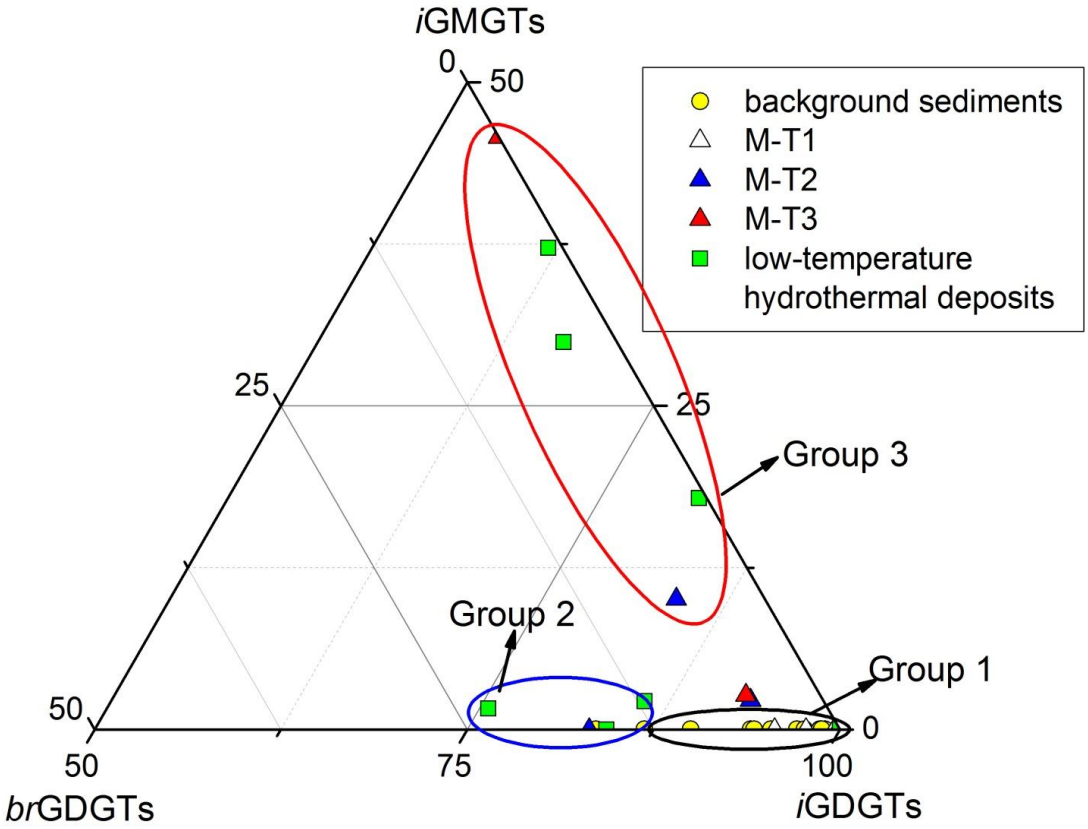

Fig. 4. Ternary diagram of *i*GDGTs, *i*GMGTs and *br*GDGTs in background and metalliferous sediments and hydrothermal deposits from the SWIR. Groups 1 to 3 were divided according to relatively higher contents of *i*GDGTs, *br*GDGTs and *i*GMGTs, respectively.

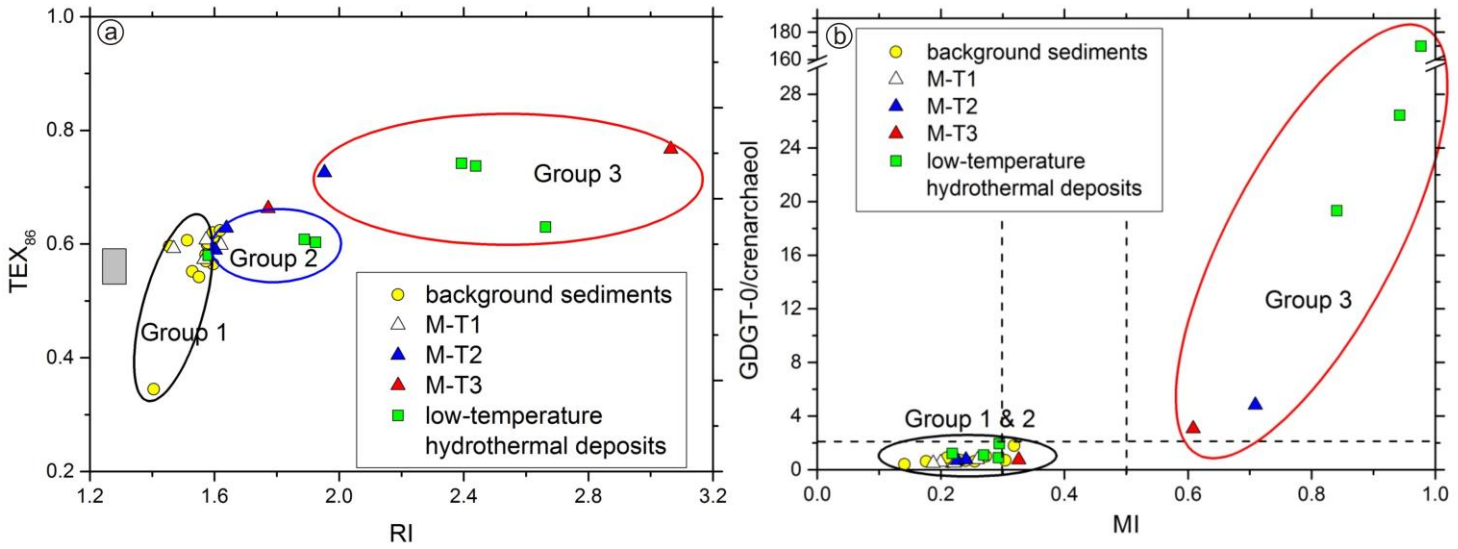

Fig. 5. Crossplots of TEX_{86} versus Ring Index (RI) (Panel a) and MI versus GDGT-0/ crenarchaeol (Panel b) in background and metalliferous sediments and hydrothermal deposits from the SWIR. In Panel a, the bar shows expected TEX_{86} values for the overlying water sea surface temperature (SST) of background sediments in the SWIR (SST in the range of 19 to 23 °C according to http://www.ospo.noaa.gov/data/sst/contour/global.c.gif, and using the TEX_{86}^{H} calibration of Kim et al., 2010, $SST=68.4\times logTEX_{86}+38.6$); note that Group 1 but also Group 2 sediments are consistent with this, whereas Group 3 are characterized by higher than expected TEX_{86} values. Both Group 2 and Group 3 exhibit elevated RIs.

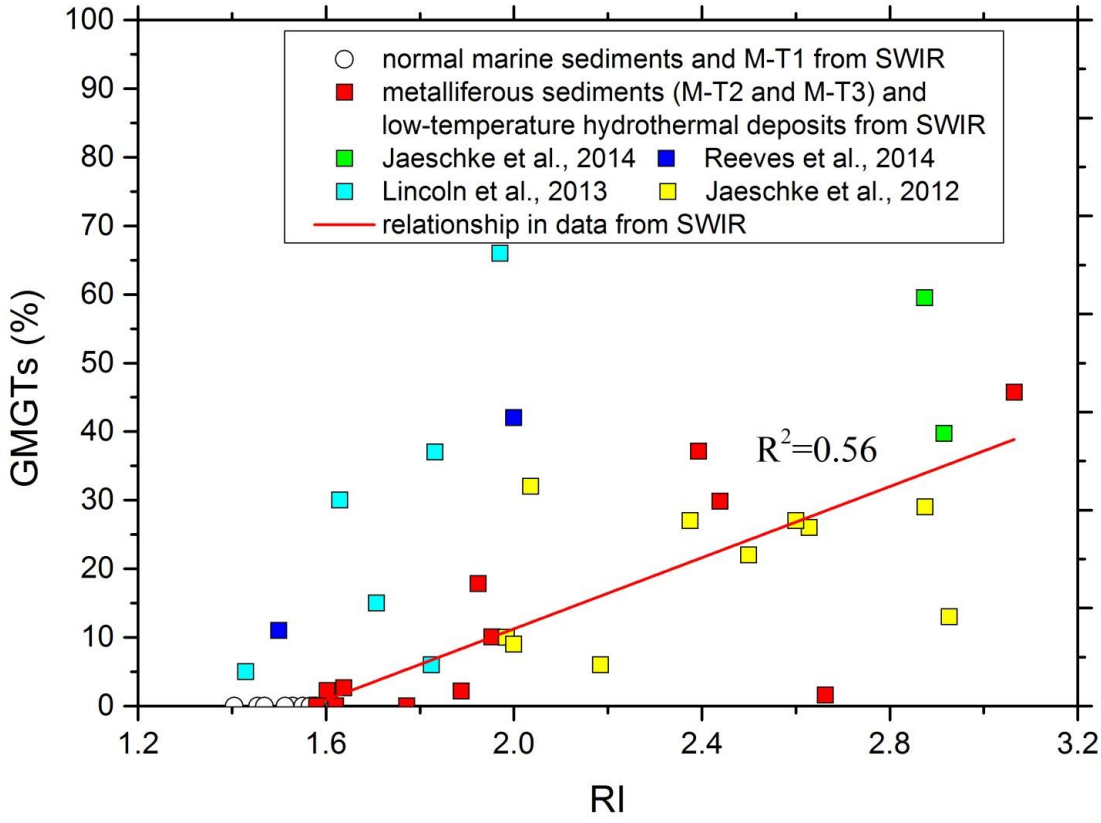

Fig. 6. Crossplot showing %GMGTs (as percentage of total tetraethers) versus RI (ring index) of background and metalliferous sediments and hydrothermal deposits from the SWIR and other hydrothermal systems. The line shows the positive relationship between GMGTs and RI in metalliferous sediments (M-T2 and M-T3) and hydrothermal deposits from SWIR, which is broadly consistent with observations from other sites. Note the several Group 1 and 2 samples with no or low GMGTs and correspondingly low RIs.

Table 1 Various tetraether lipid-based parameters for background sediments, metalliferous sediments and low-temperature hydrothermal deposits from the SWIR.

Type	No.	*i*GDGTs (%)	*i*GMGTs (%)	*br*GDGTs (%)	MBT	CBT	BIT	GDGT-0/ Crenarchaeol	RI	TEX_{86}	MI	*i*GMGTs/ *i*GDGTs	Group
background sediments	SW6	100	0.00	0.00	—	—	0.00	0.75	1.5	0.55	0.22	0.00	
	SW7	95	0.00	5.0	0.16	-0.11	0.05	0.63	1.6	0.60	0.26	0.00	
	SW9	97	0.00	3.0	0.11	-0.11	0.05	0.71	1.6	0.54	0.30	0.00	
	SW11	99	0.00	1.0	0.00	—	0.02	0.42	1.5	0.61	0.14	0.00	
	SW12	87	0.00	13	0.11	-0.12	0.19	1.0	1.6	0.58	0.27	0.00	
	SW13	98	0.00	2.0	0.09	-0.19	0.03	0.70	1.6	0.61	0.23	0.00	
	SW17	90	0.00	10	0.17	0.17	0.12	0.62	1.5	0.60	0.18	0.00	1
	SW19	99	0.00	1.0	0.13	-0.49	0.01	0.71	1.6	0.56	0.22	0.00	
	SW20	94	0.00	6.0	0.11	0.35	0.10	0.67	1.6	0.61	0.24	0.00	
	SW21	84	0.00	16	0.14	0.14	0.31	1.8	1.4	0.35	0.32	0.00	
	SW22	94	0.00	6.0	0.00	-0.42	0.06	0.59	1.6	0.60	0.21	0.00	
	SW27	99	0.00	1.0	0.27	—	0.03	0.90	1.6	0.57	0.21	0.00	
	SW28	99	0.00	1.0	0.04	0.10	0.02	0.72	1.6	0.62	0.23	0.00	
M-T1	SW2	100	0.00	0.00	0.14	0.44	0.01	0.52	1.6	0.62	0.22	0.00	
	SW3	96	0.00	4.0	0.00	0.12	0.06	0.56	1.5	0.59	0.20	0.00	1
	SW4	98	0.00	2.0	0.00	0.28	0.03	0.50	1.6	0.61	0.19	0.00	
	SW10	100	0.00	0.00	0.00	—	0.00	0.76	1.6	0.57	0.26	0.00	
M-T2	SW32	83	0.00	17	0.44	1.06	0.28	0.71	1.6	0.60	0.23	0.00	2
	SW38	84	10	6.0	0.30	0.12	0.26	4.8	2.0	0.73	0.71	0.12	3
	SW39	93	2.2	4.8	0.28	0.25	0.07	0.76	1.6	0.59	0.24	0.02	n.d.
M-T3	SW35	92	2.7	5.0	0.15	-0.35	0.05	0.75	1.6	0.63	0.33	0.03	n.d.
	SW40	54	46	0.00	—	—	0.00	3.1	3.1	0.77	0.61	0.84	3
low-temperature hydrothermal deposits	SW31	100	0.00	0.00	—	—	0.00	2.0	1.8	0.66	0.29	0.00	n.d.
	SW33	76	1.6	23	0.69	0.04	0.26	0.89	2.7	0.63	0.29	0.02	2
	SW36	84	0.00	16	0.06	-0.28	0.26	1.2	1.6	0.58	0.22	0.00	2
	SW37	82	18	0.52	1.0	—	0.24	26	1.9	0.60	0.94	0.22	3
	SW41	86	2.2	12	0.32	0.83	0.24	1.1	1.9	0.61	0.27	0.03	2
	SW45	66	30	3.6	0.22	0.05	0.42	19	2.4	0.74	0.84	0.45	3
	SW46	62	37	0.94	0.30	0.34	0.69	170	2.4	0.74	0.98	0.60	3

— Some of the components involved in the index were not detected, precluding its calculation.

n.d., not determined; these samples were distinct from Group 1, but not characterized by the defining features of either Group 2 or Group 3.